

Terahertz Spectroscopy Applications

(non-biological)

17 December 2009



THz spectroscopy has been used to study:

(amongst others, and in no particular order)

- Polymers
- Semiconductors
- Ceramics and glasses
- Organic molecules
- Gas spectroscopy
- Conductive films
- Liquid crystals
- Composites
- Oils
- Nondestructive testing

Polymers

(*non-polar!*)

Non-polar, e.g.:

PTFE (Teflon)

Polyethylene

Polypropylene

Polar, e.g.:

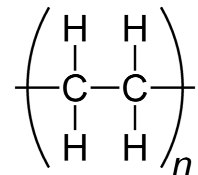
Polystyrene

Perspex

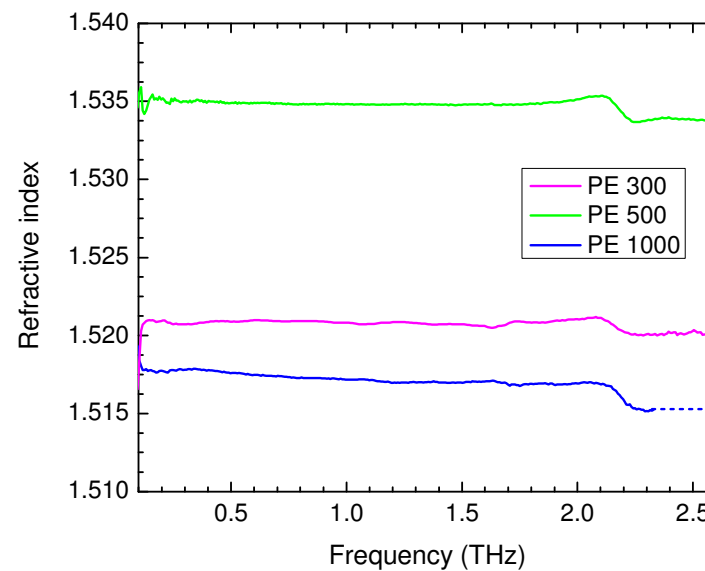
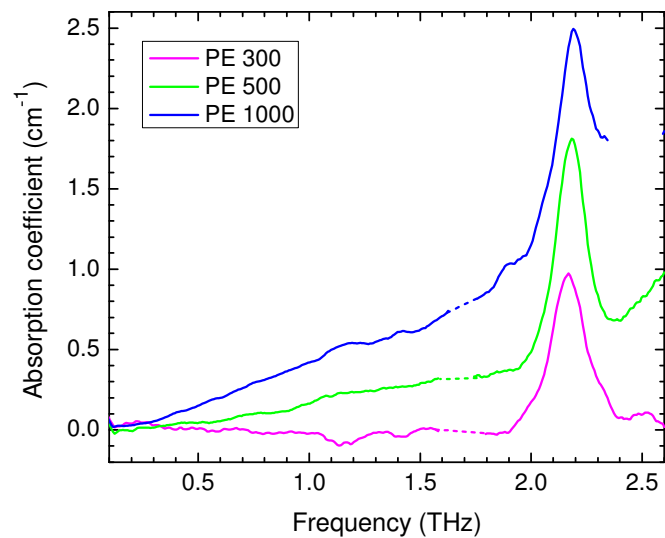
Vinyl

- Observing polymerisation
- Differentiating polymorphs
- Measuring electrical conductivity
- Measuring hygroscopicity

Effect of chain length in polyethylene

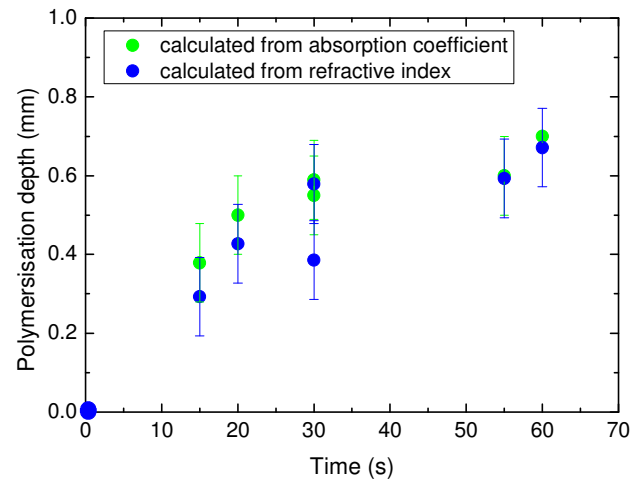
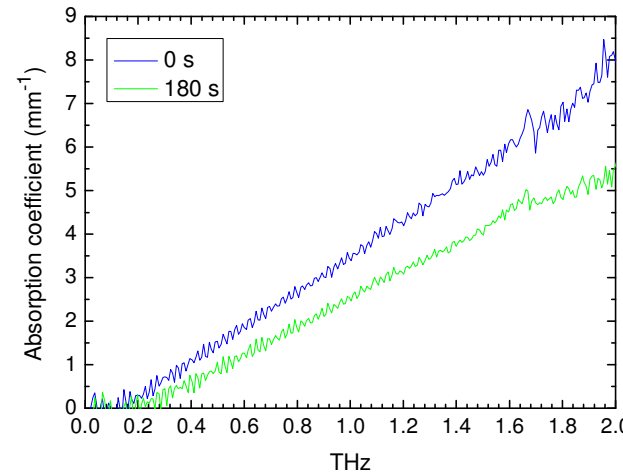
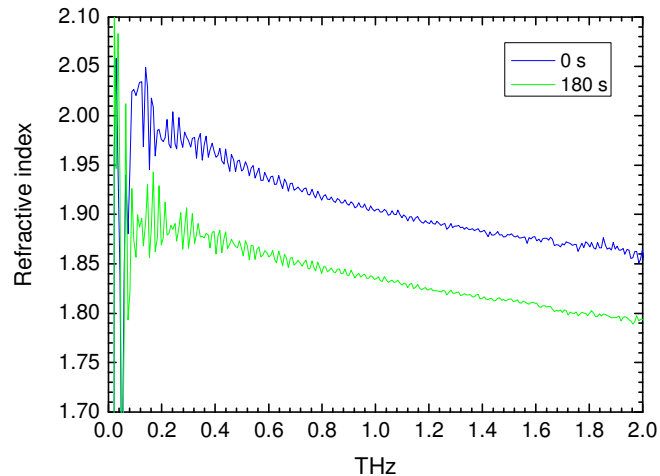


Polyethylene monomer



Polymerisation in SU8

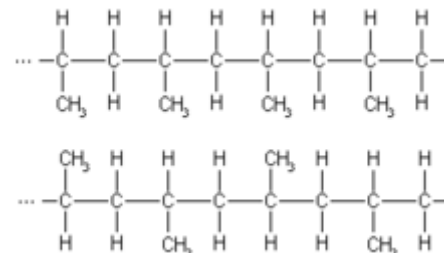
SU8 is an epoxy resin used as a UV-curable photoresist



Propagation of the polymerisation front

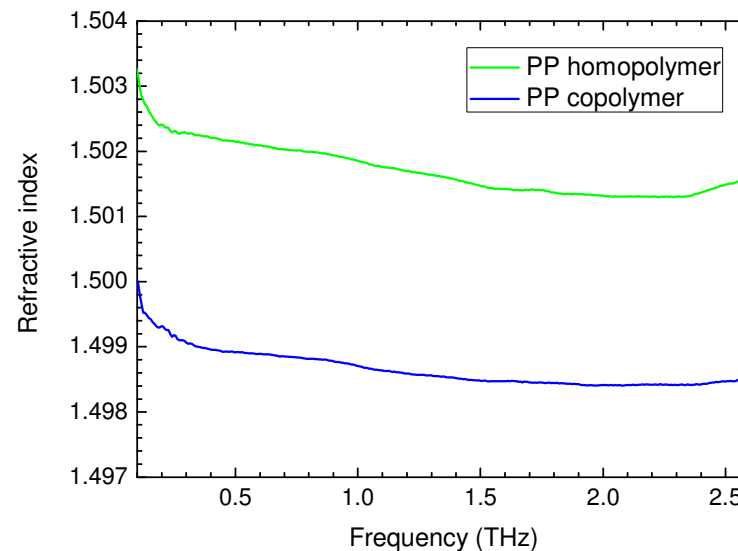
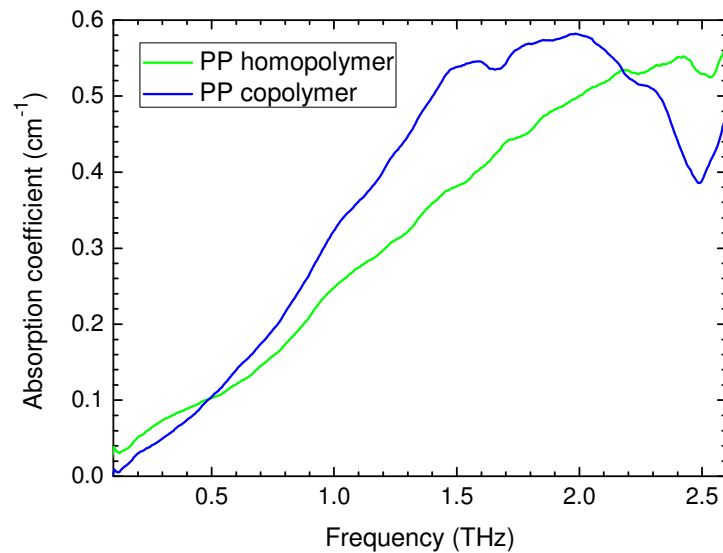
Differentiating polymorphs

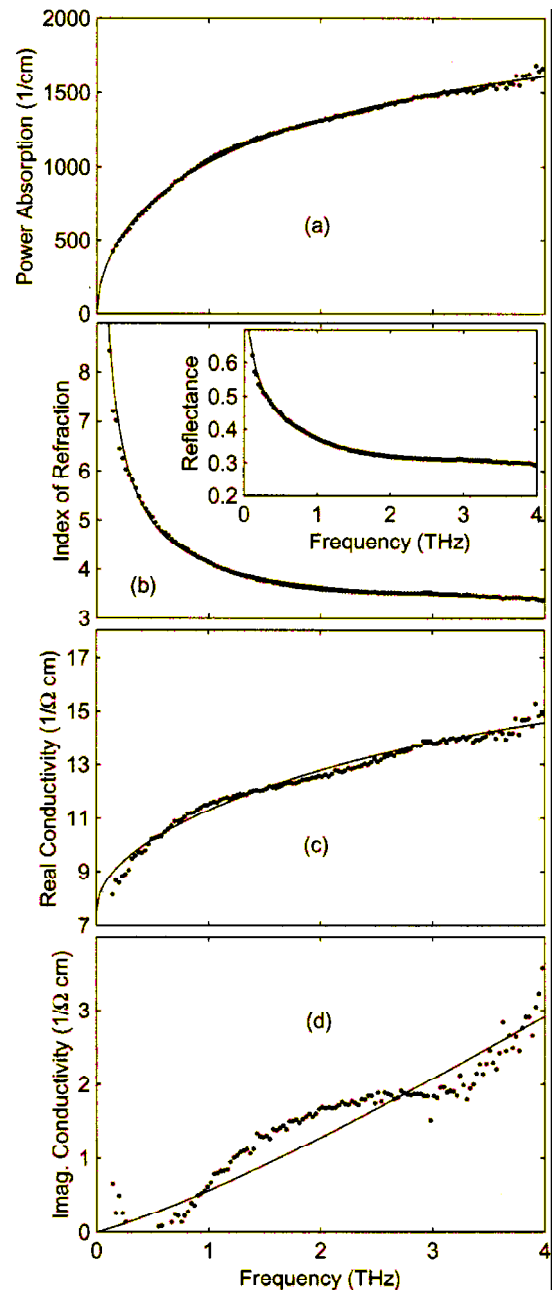
Polypropylene



Isotactic

Syndiotactic





Characterization of conducting poly-3-methylthiophene film

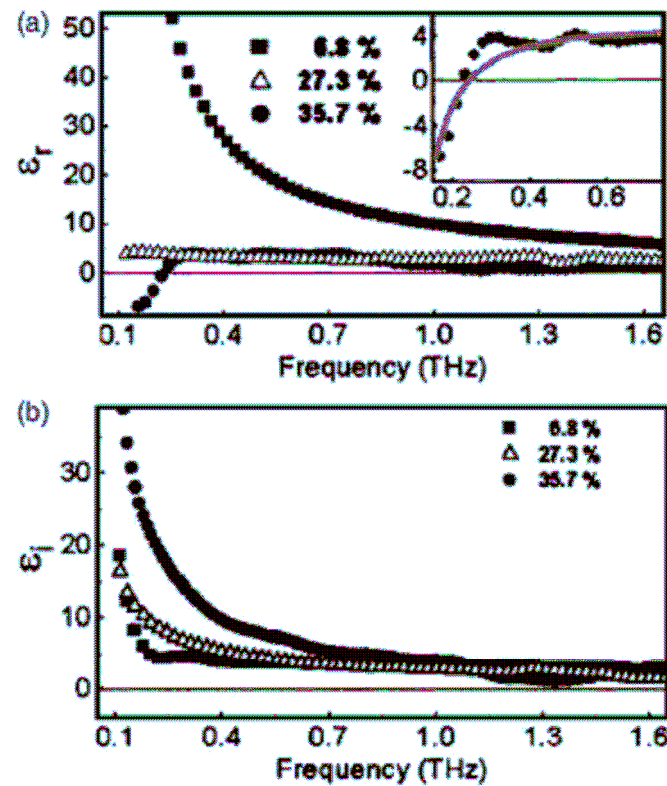
TI Jeon et al, Appl. Phys. Lett. **79**/25 (2001) 4142-4144

In this conducting polymer absorption and refractive index are mostly due to the free carriers.

(solid line: Drude model)

Observing the metal-insulator transition in PMMA-graphite composite (polymethylmethacrylate)

AM Seo et al, J. Appl. Phys., **99**, 066103 (2006)



By varying the graphite content it is possible to engineer the dielectric constant of the material in order to manufacture absorbers with a wide range of shielding.

Measuring hygroscopicity of polymers

J. Balakrishnan et al, Appl. Opt., 48/12 (2009) 2262-2266

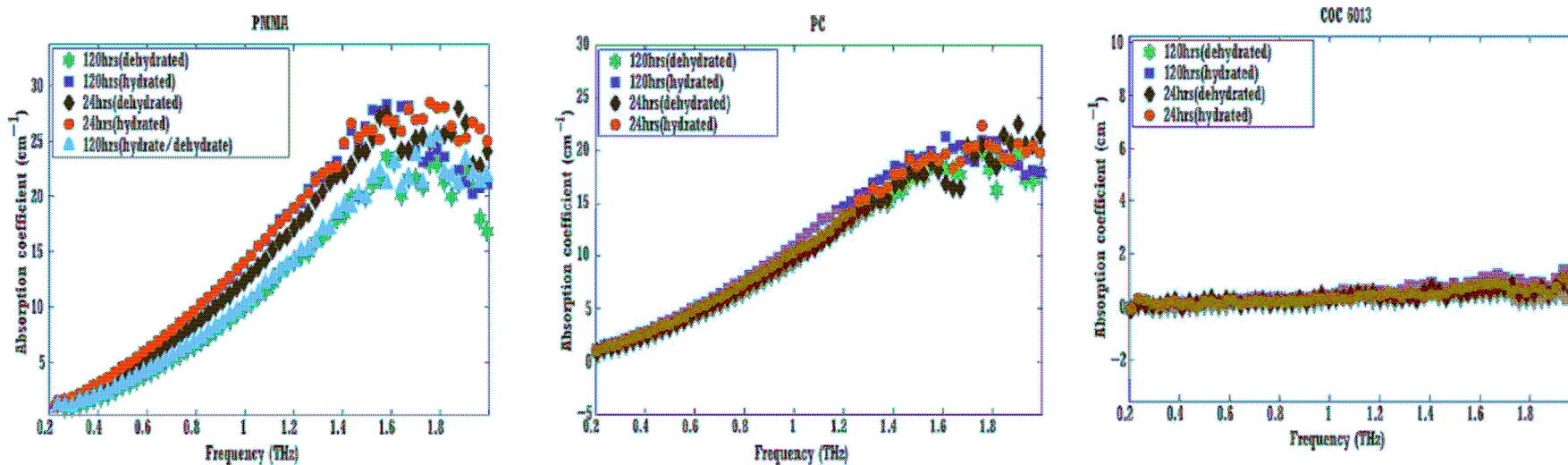


Table 1. Variation in Absorption Coefficient and Hygroscopicity of Polymer Materials for 24 h and 120 h Measurements at 1 THz^a

	Polymer	Absorption (cm ⁻¹)				Hygroscopicity (%)			
		24 h		120 h		Experimental		Literature	
		Hydrated	Dehydrated	Hydrated	Dehydrated	24 h	120 h	24 h [28]	120 h
non-polar	COC 6013	0.269	0.240	0.361	0.160	0.01	0.09	0.01	—
	COC 5013	0.334	0.315	0.485	0.290	0.01	0.08	0.01	—
	HDPE	0.259	0.215	—	—	0.02	—	0.01	—
	PTFE	—	—	0.552	0.450	—	0.04	0.01	—
polar	PMMA	14.020	12.393	14.015	10.000	0.75	1.80	0.5	—
	PVC	22.218	22.087	22.263	21.998	0.06	0.11	0.06	—
	PC	10.346	9.800	10.977	9.457	0.21	0.69	0.25	—

^aHygroscopicity data obtained from Eq. (7) are compared with the standard test method for water absorption of polymers (ASTM D570) to verify agreement.

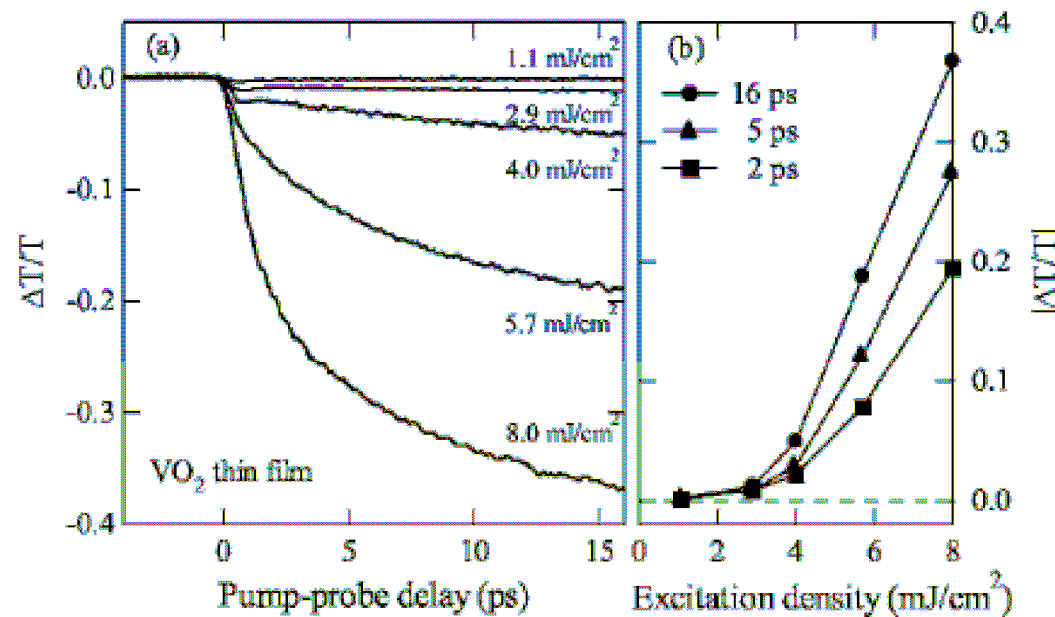
Semiconductors

- Carrier dynamics
- Electron mobilities
- Quantum dot properties
- Fault inspection

Studied by using optical pump and THz probe

Photoinduced metallic state in VO₂ using optical pump, THz probe

M. Nakajima et al., Appl. Phys. Lett. **92**, 011907 (2008)



Temporal dependence of THz transmittance

Electron mobility in GaAs alloys

DG Cooke et al, Appl. Phys. Lett. **89**, 122103 (2006)

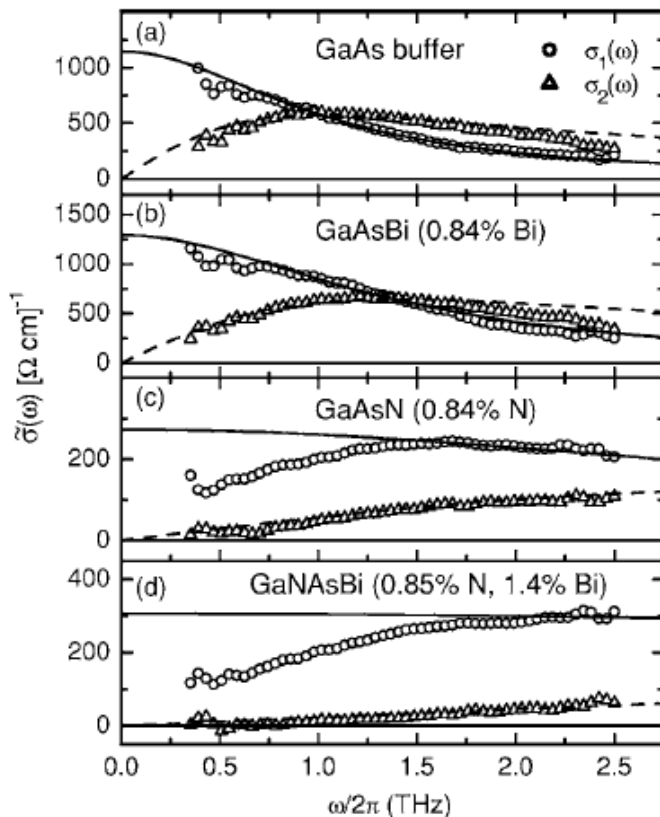


FIG. 2. Extracted complex conductivity for (a) GaAs buffer layer, (b) GaAsBi (0.84% Bi) (c) GaNAs (0.84% N), and (d) GaNAsBi (0.85% N, 1.4% Bi) 10 ps after 400 nm excitation at a fluence of $3.7 \mu\text{J}/\text{cm}^2$. The solid and dashed lines are fits to the real and imaginary parts of the Drude conductivity with (a) $\omega_p/2\pi=46\pm1 \text{ THz}$, $\tau=157\pm7 \text{ fs}$, (b) $\omega_p/2\pi=57\pm1 \text{ THz}$, $\tau=115\pm4 \text{ fs}$, (c) $\omega_p/2\pi=48\pm2 \text{ THz}$, $\tau=35\pm3 \text{ fs}$, and (d) $\omega_p/2\pi=86\pm2 \text{ THz}$, $\tau=12\pm1 \text{ fs}$.

TABLE I. Extracted electron mobilities from Drude fits to the complex conductivity in various samples for early delay times $\Delta t=4-10 \text{ ps}$, with a 400 nm pump fluence of $3.7 \mu\text{J}/\text{cm}^2$ ($n \sim (2-3) \times 10^{18} \text{ cm}^{-3}$).

Sample	$\mu_e (\text{cm}^2/\text{V s})$
GaAs buffer layer	3300 ± 100
$\text{GaAs}_{1-y}\text{Bi}_y$ ($y=0.84\%$)	2800 ± 100
$\text{GaAs}_{1-y}\text{Bi}_y$ ($y=1.0\%$, AlGaAs barrier)	2800 ± 100
$\text{GaAs}_{1-y}\text{Bi}_y$ ($y=1.4\%$)	2700 ± 100
$\text{GaN}_x\text{As}_{1-x}$ ($x=0.84\%$)	920 ± 80^a
$\text{GaN}_x\text{As}_{1-x-y}\text{Bi}_y$ ($x=0.85\%$, $y=1.4\%$)	340 ± 30^a

^aDerived from high frequency fits to the Drude model.

Electron-to-Hole Energy Transfer in CdSe Quantum Dots

E Hendry et al, Phys. Rev. Lett. **96**, 057408 (2006)

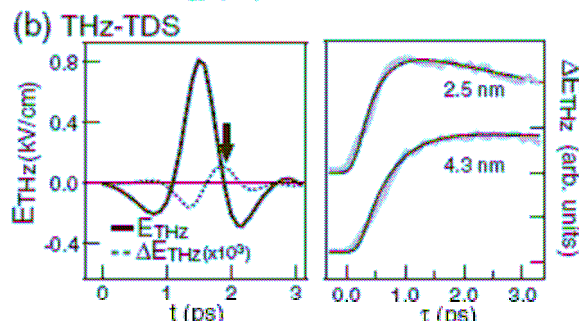
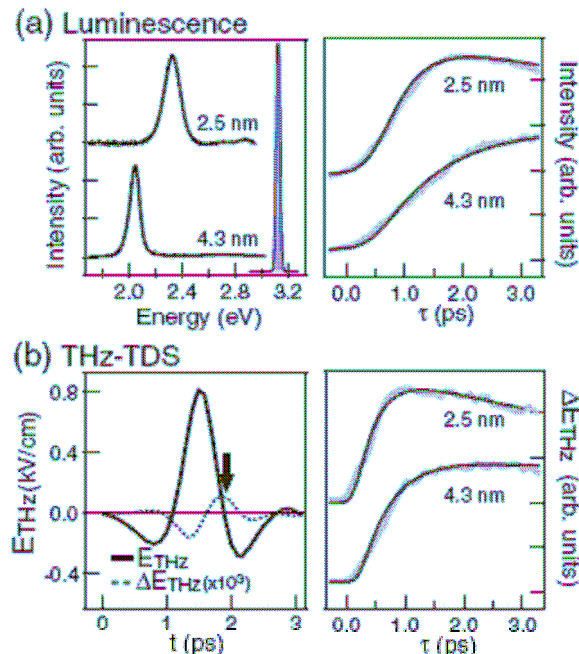
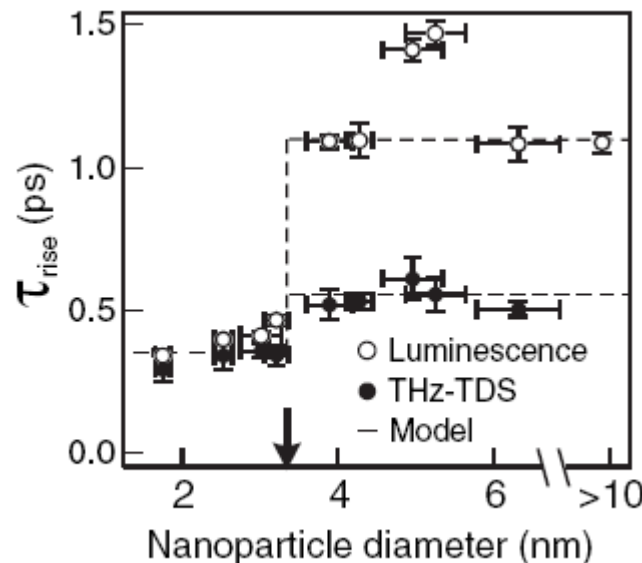


FIG. 1. (a) Left: Luminescence spectra. Also shown is the excitation pulse (shaded area). Right: We measure the increase in intensity at the peak of the luminescence spectra (gray lines) as a function of delay τ . (b) Left: The transmitted THz pulses $E_{\text{THz}}(t, \tau)$ and the exciton-induced modulation thereof, $\Delta E_{\text{THz}}(t, \tau)$. Right: The modulation is measured at the point marked with an arrow in the left panel ($t = 1.9$ ps), as a function of τ , giving rise to the transient hole population of the $1S_{3/2}$ level. The dynamics in both (a) and (b) are adequately described by exponential rise times determined by the carrier cooling rates (black lines in the right-hand panels).



Inspection for electrical failures in semiconductor devices

M. Yamashita et al., Appl. Phys. Lett. **93**, 041117 (2008)

Terahertz pulses are generated from nonbiased Si-MOSFETs by exciting *p-n* junctions with ultrafast laser pulses. The waveforms of terahertz pulses depend on the interconnection structure near the *p-n* junctions. Defects in the circuit wiring give rise to changes in the terahertz emission images.

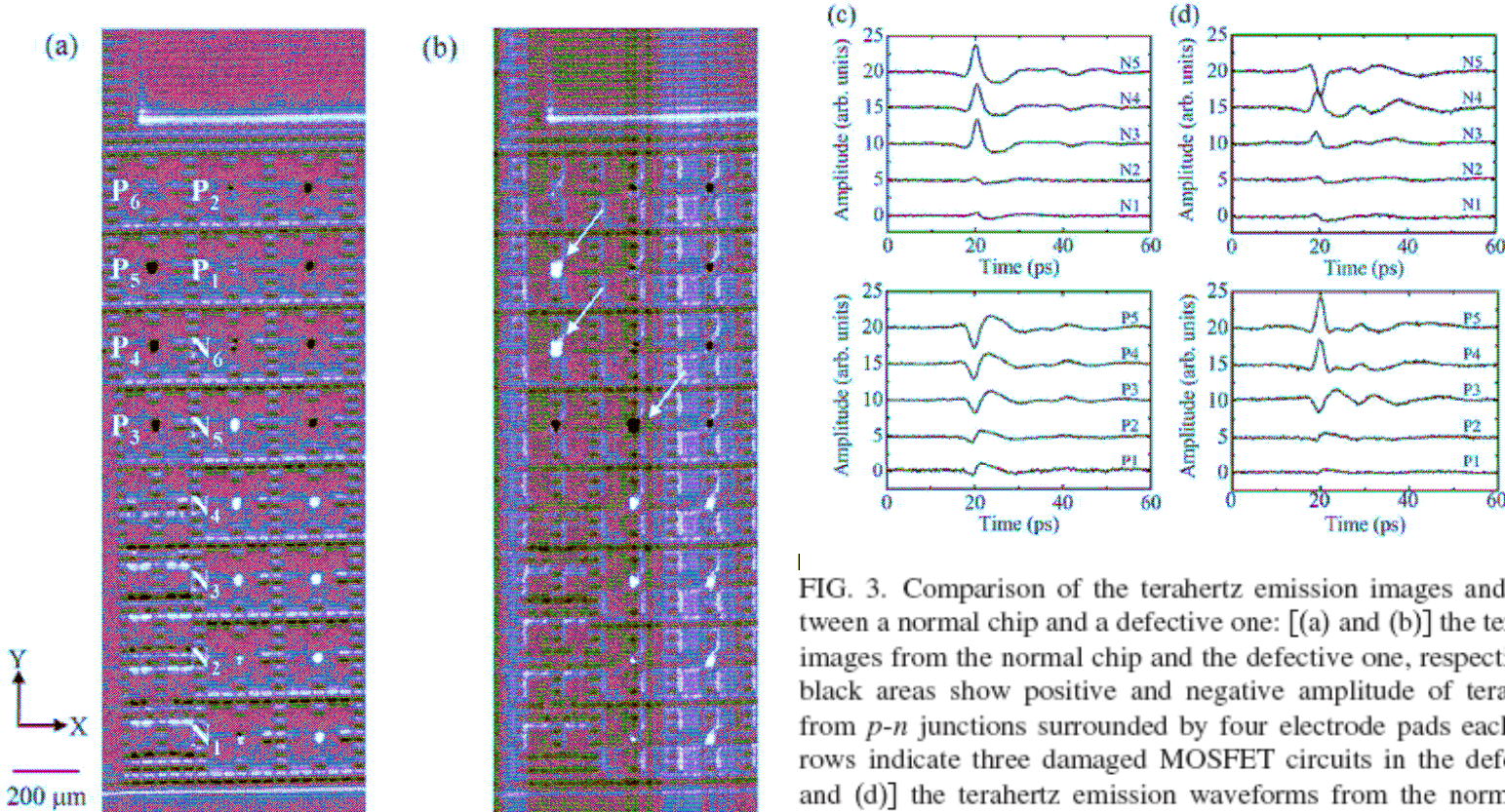


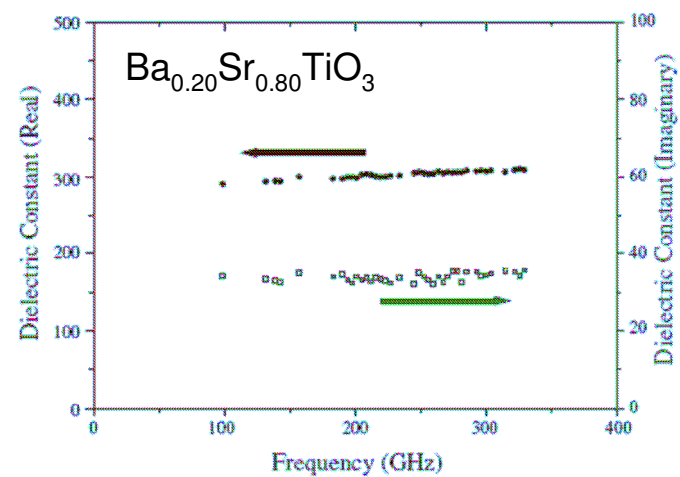
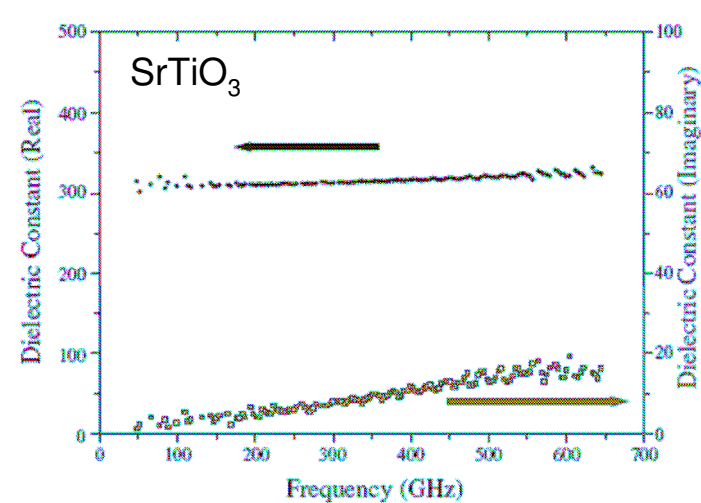
FIG. 3. Comparison of the terahertz emission images and waveforms between a normal chip and a defective one: [(a) and (b)] the terahertz emission images from the normal chip and the defective one, respectively. White and black areas show positive and negative amplitude of terahertz emissions from *p-n* junctions surrounded by four electrode pads each. The white arrows indicate three damaged MOSFET circuits in the defective chip; [(c) and (d)] the terahertz emission waveforms from the normal chip and the defective one, respectively.

Ceramics and Glasses

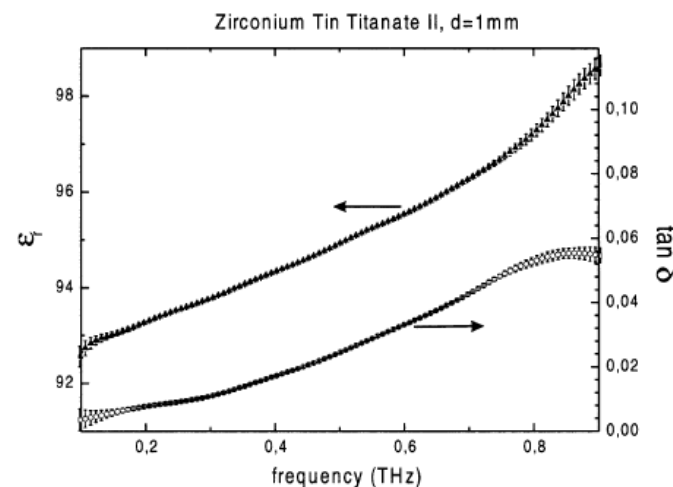
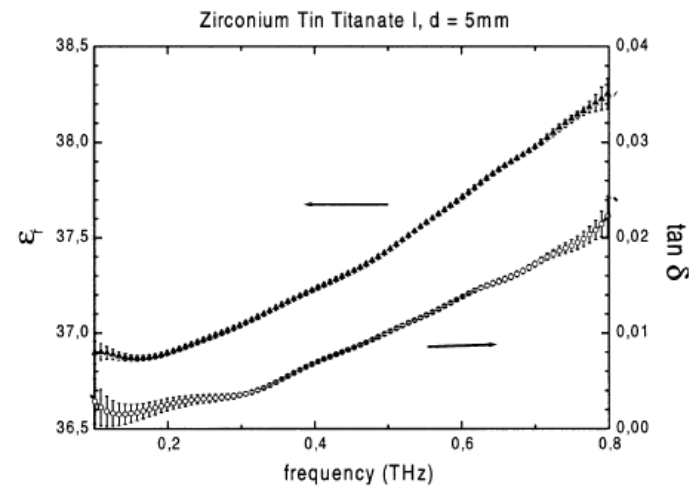
- Characterisation
- Relationship with material properties

High dielectric constant ceramics

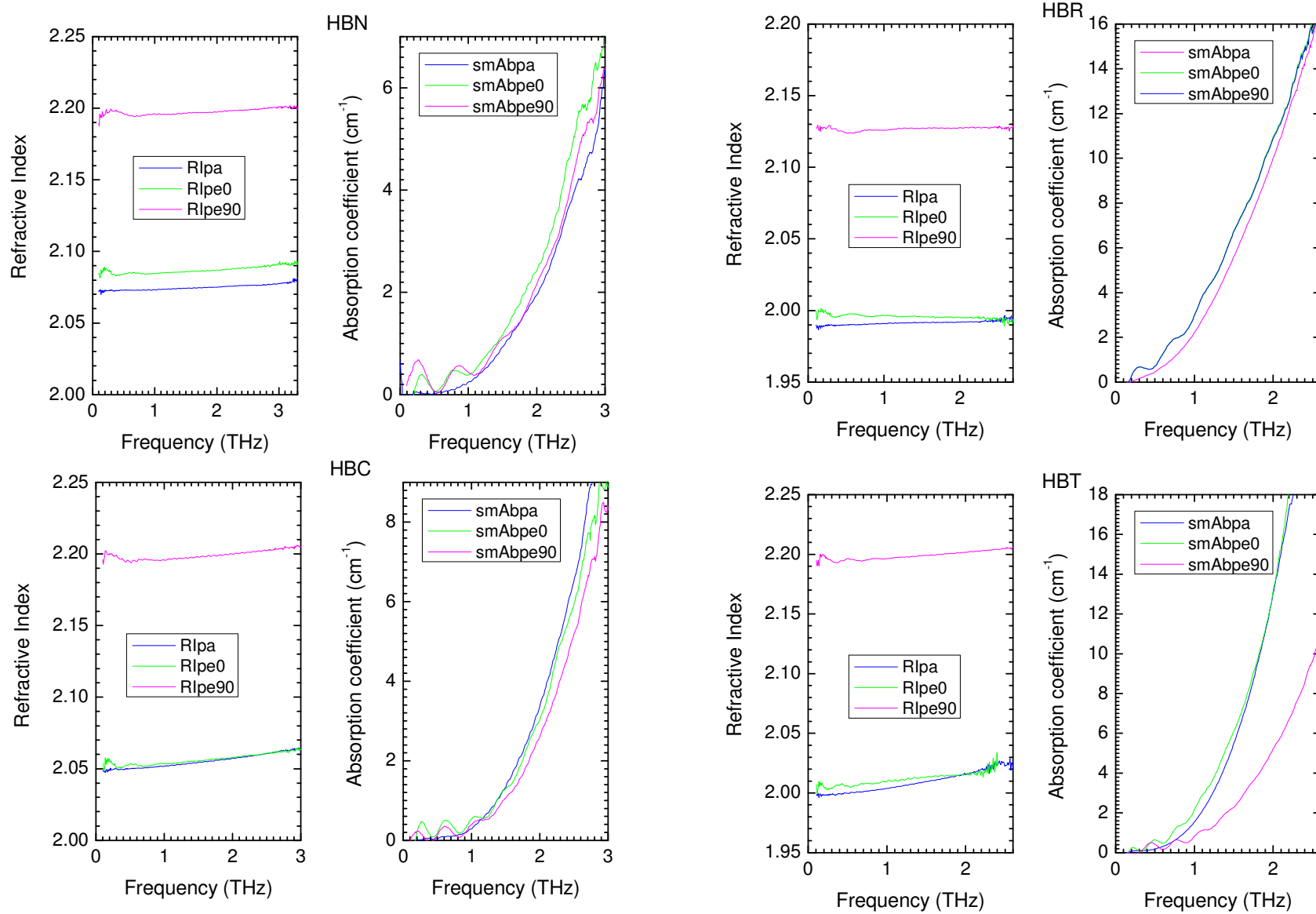
T Fuji et al, Jap. J. Appl. Phys.
43/9B (2004) 6765–6768



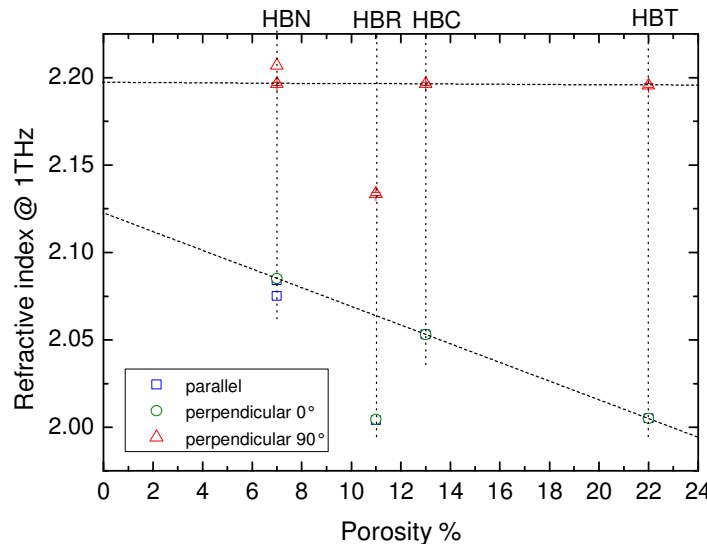
PH Bolivar, IEEE Trans. MTT
51/4 (2003), 1062-1066



Different grades of Boron Nitride

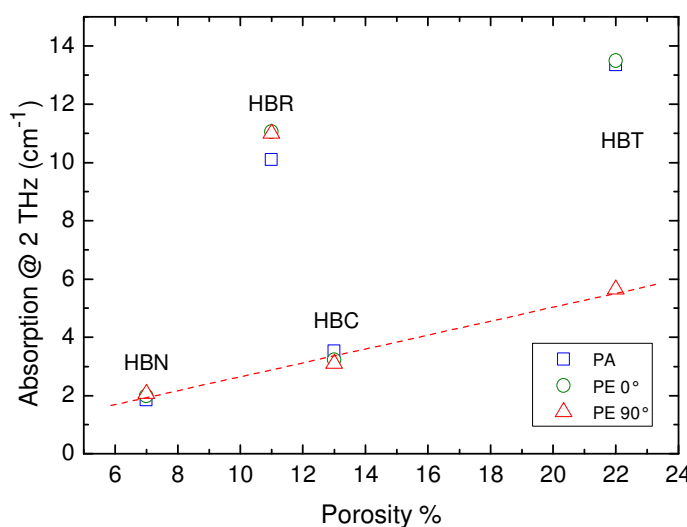


Relationship with Boron Nitride properties



Boron Nitride (BN)
is birefringent
and dichroic

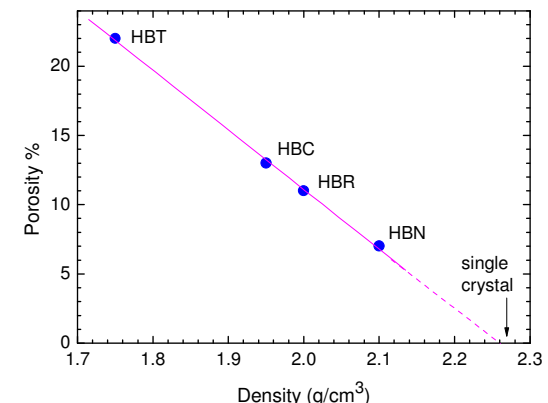
Crystals are
oriented
along the
pressing axis



n_o decreases with porosity
 n_e remains constant

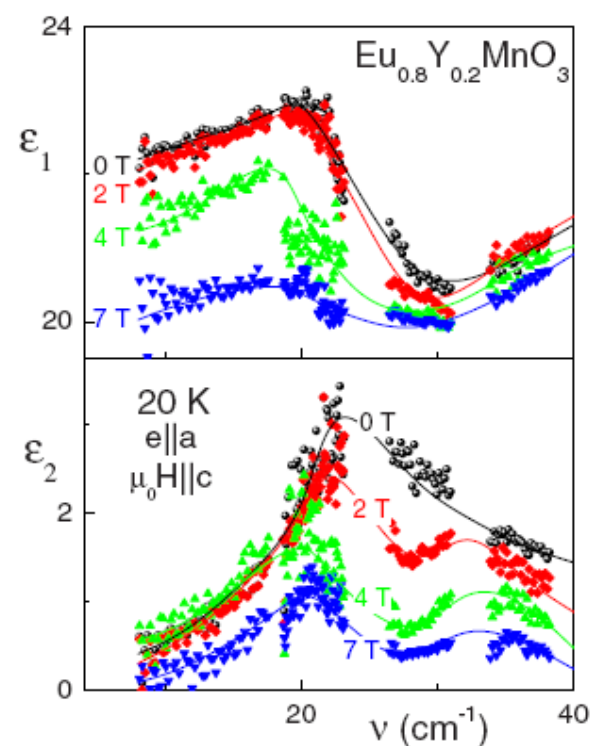
O-ray absorption
increases faster
than E-ray

Conclusion: porosity between
platelets is anisotropic,
oriented along the O-axis

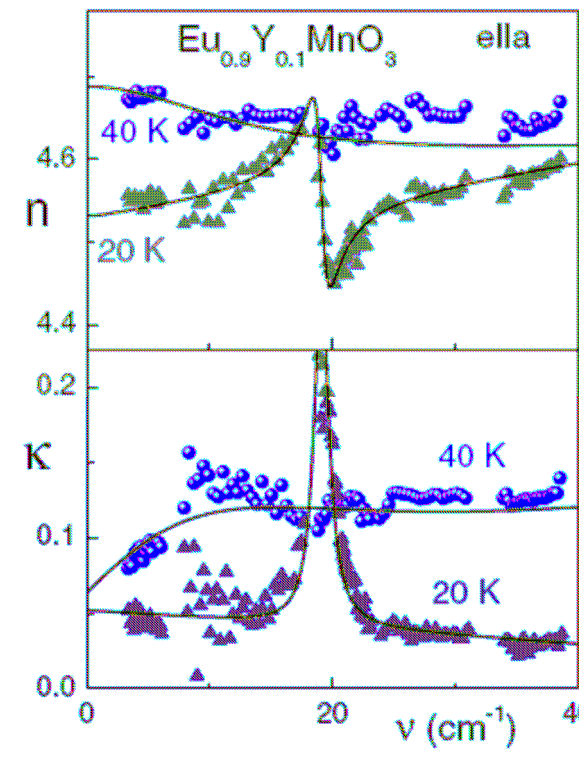


Magnetoelectric contributions to the permittivity of $\text{Eu}_{1-x}\text{Y}_x\text{MnO}_3$

A. Pimenov et al., Phys. Rev. B 77, 014438 2008

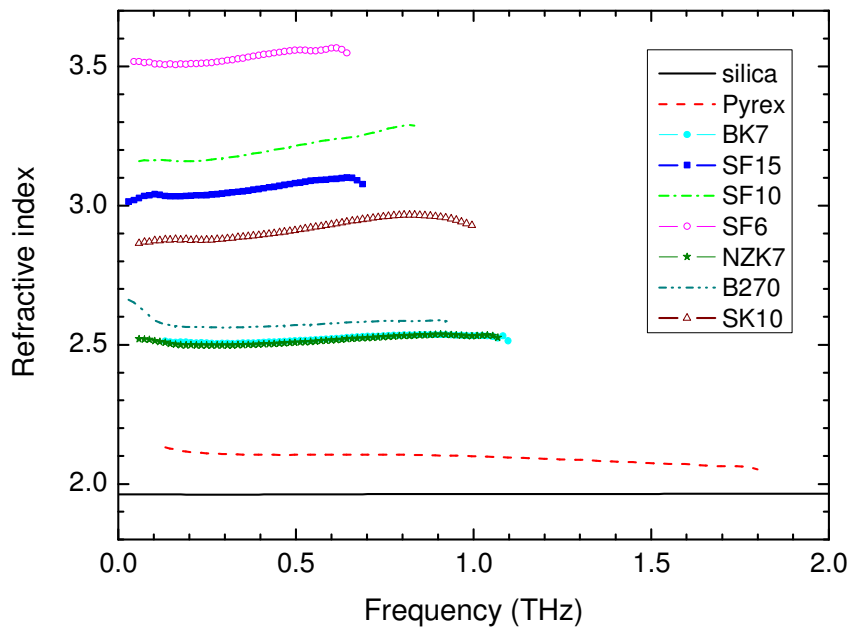
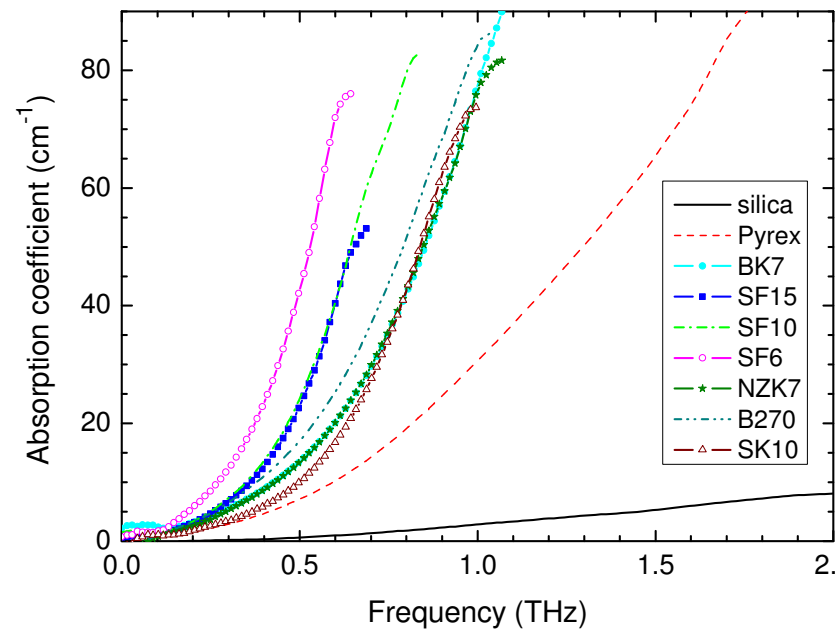


Magnetoelectric effect

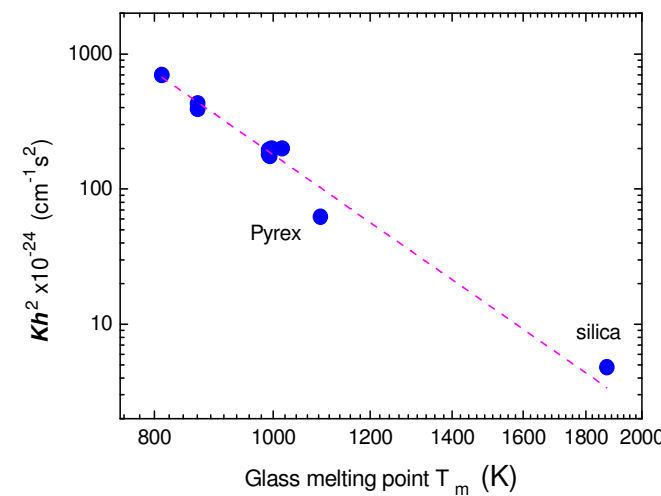
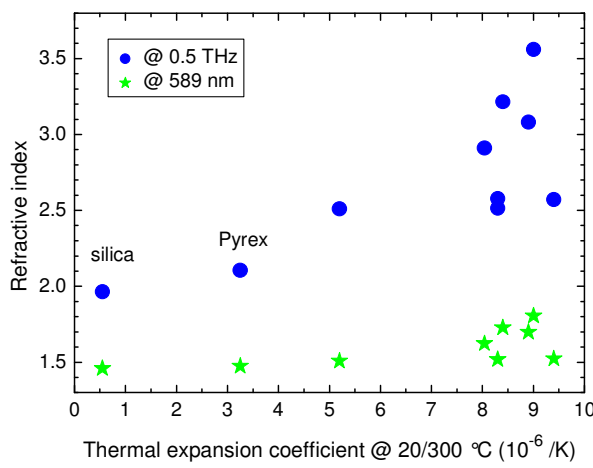
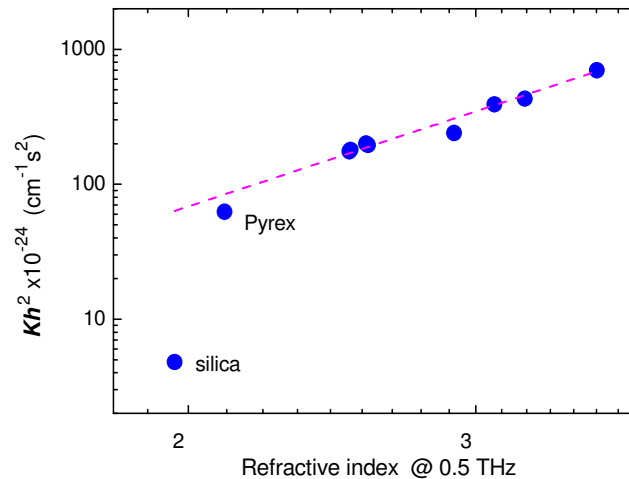
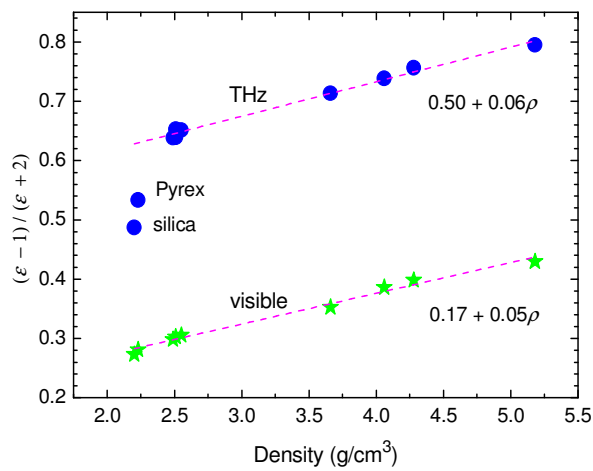


Antiferromagnetic resonance

Silicate glasses (Schott)



Silicate glasses relationship with material properties



Liquid Crystals

- Dielectric properties
- Conductivity
- Mixtures and colloids

Liquid crystal colloid with SiO_2

40-n-pentyl-4-cyanobiphenyl (5CB)

M Ohe et al, Mol. Cryst. Liq. Cryst., **480**, 21–28 (2008)

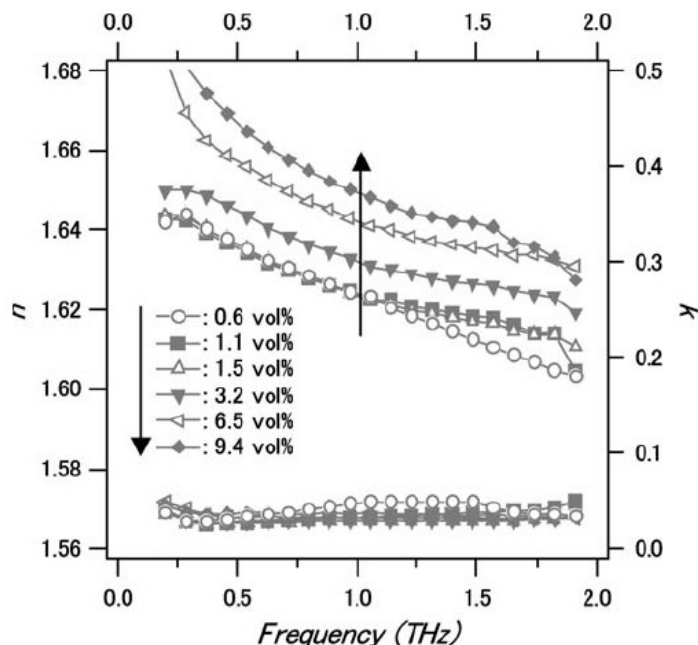


FIGURE 1 THz frequency dependence of the refractive index $n(f)$ and the absorption coefficient $k(f)$ as a function of SiO_2 particle volume fraction.

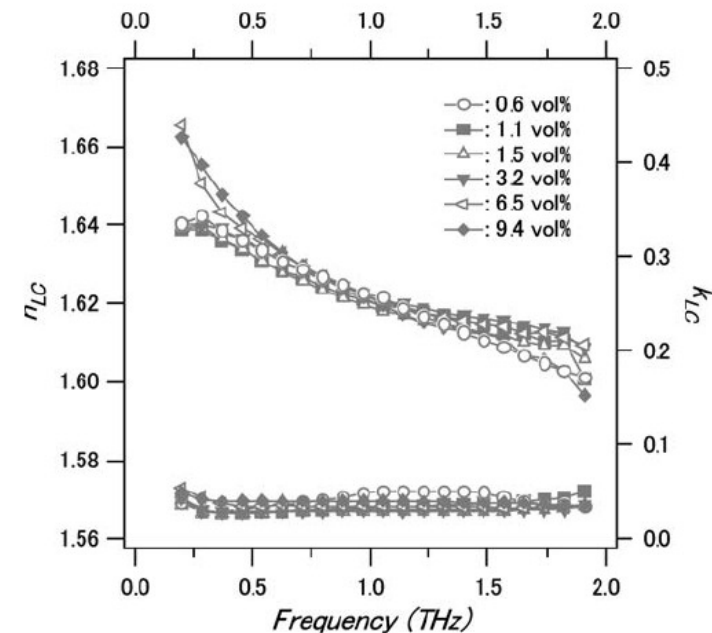
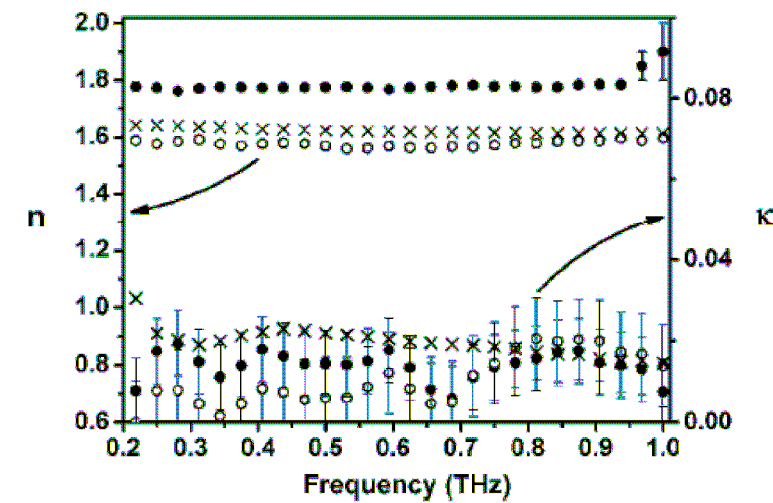
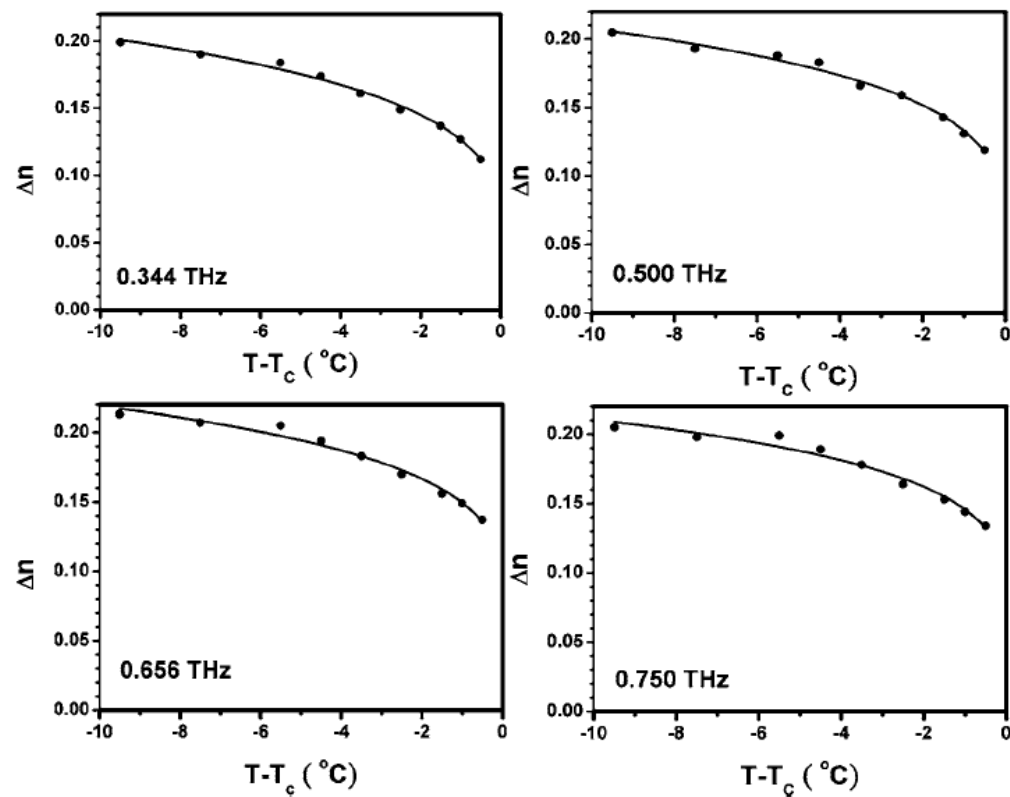


FIGURE 3 THz frequency dependence of the refractive index $n_{LC}(f)$ and the absorption coefficient $k_{LC}(f)$ extracted using effective medium theory as a function of SiO_2 particle volume fraction.

Temperature-dependent optical properties

40-n-pentyl-4-cyanobiphenyl (5CB)

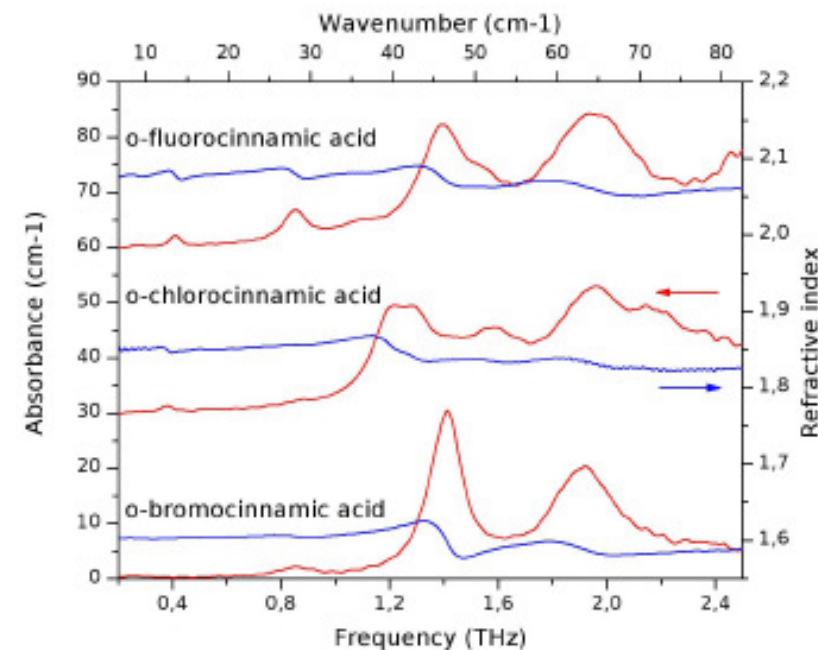
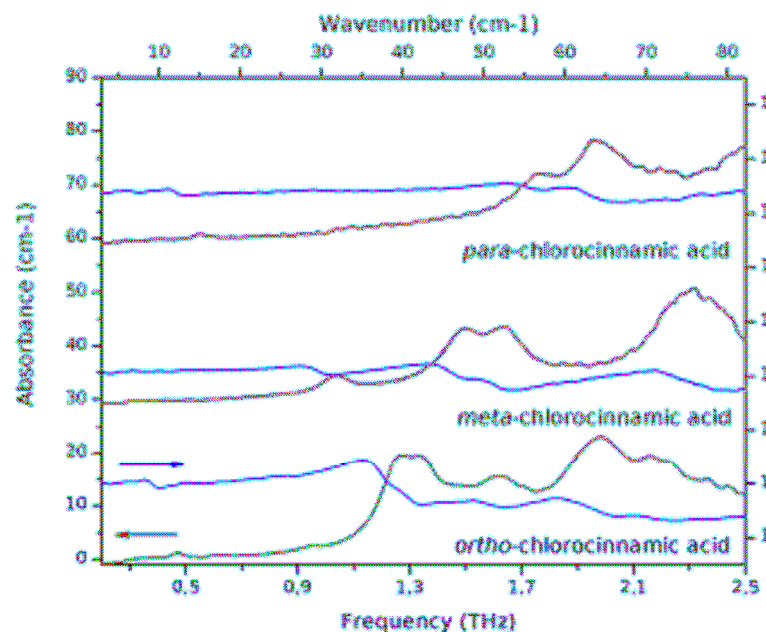
RP Pan et al, J. Appl. Phys. **103**, 093523 (2008)



Differentiating polymorphs of organic molecules

Polymorphs of acids

P. Fromentin et al, 978-1-4244-2120-6/08/\$25.00 ©IEEE.



Temperature- Induced Phase Transitions in Polymorphic Forms of Sulfathiazole

JA Zeitler et al, J. Pharm.Sci.
95/11 (2006) 2486-2498

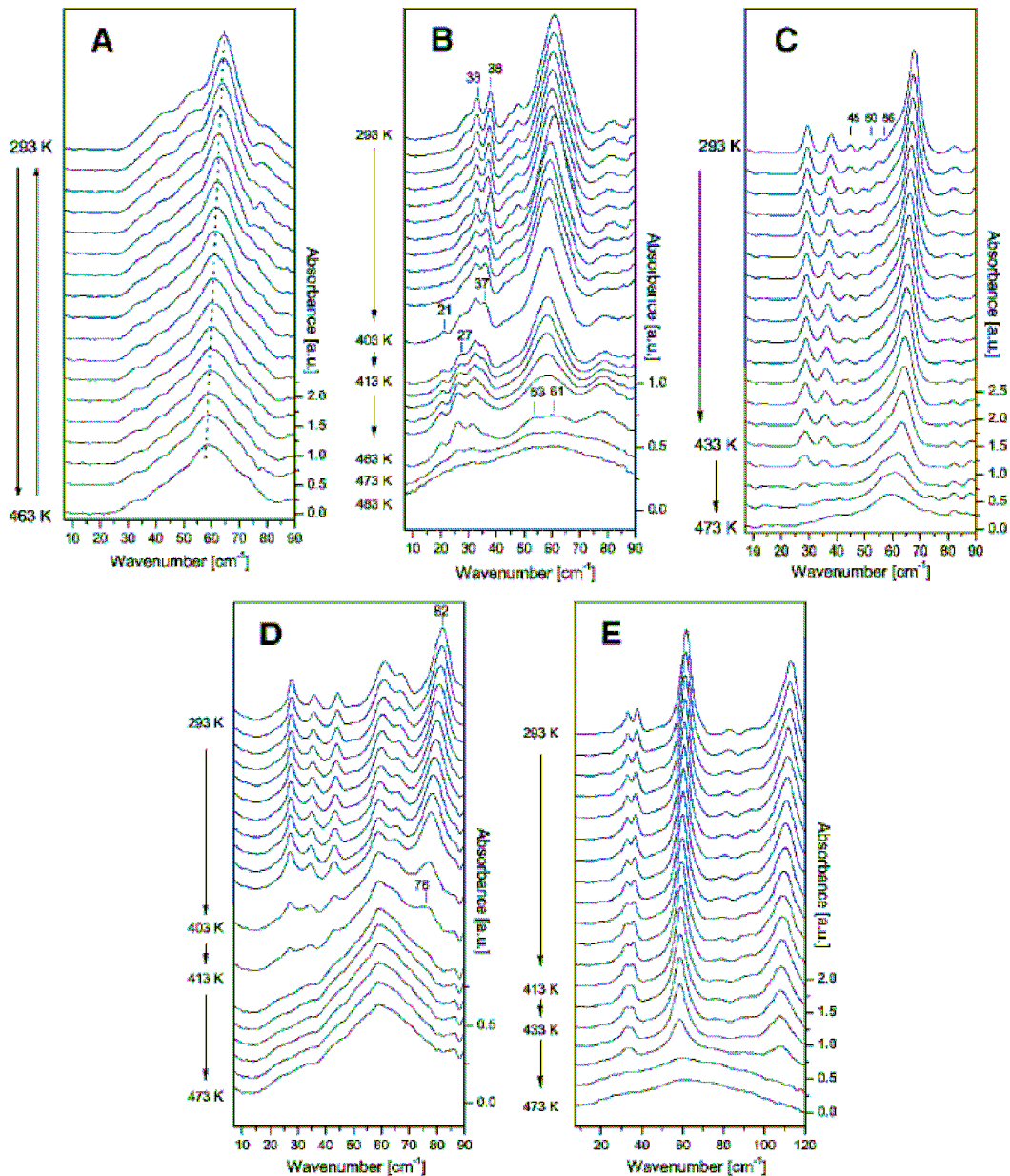
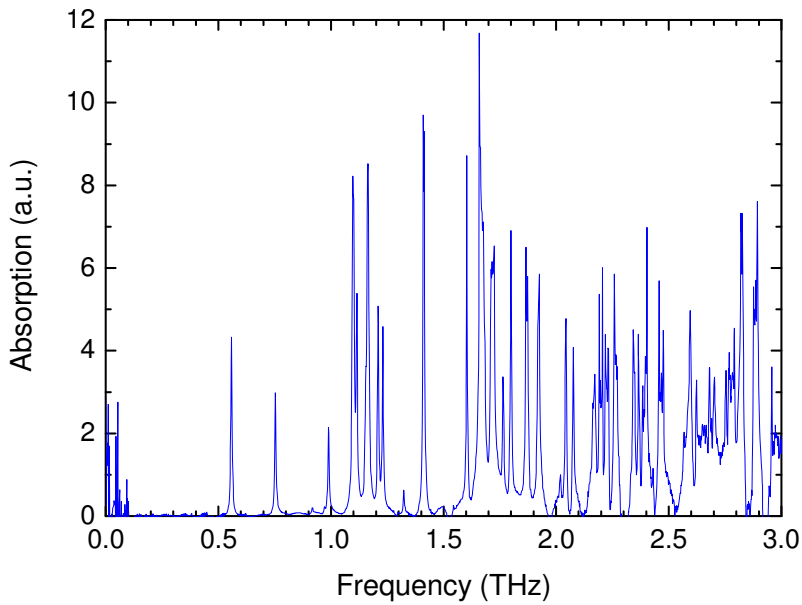


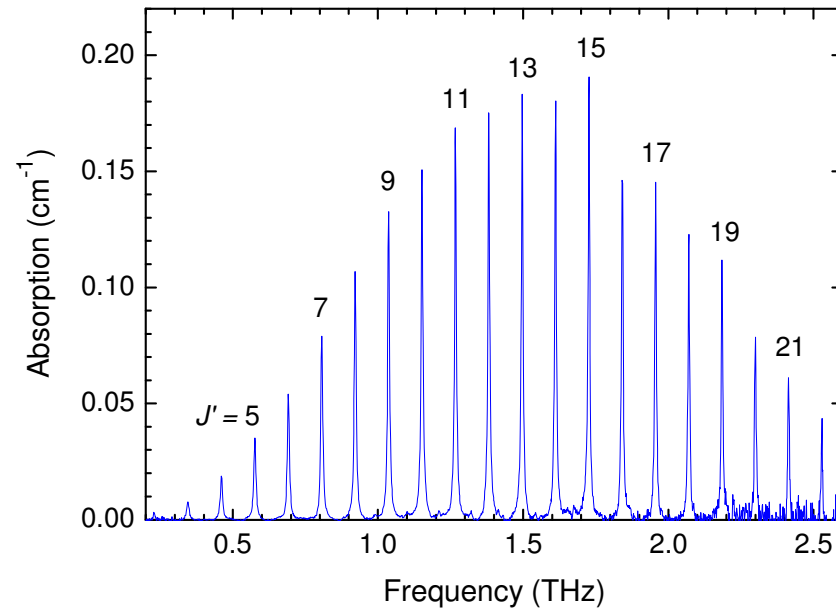
Figure 8. Sulfathiazole forms I, II, III, IV, and V. (A) Form I heating from 293 to 463 K and subsequent cooling back to room temperature. Heating from room temperature to 473 K: (B) form II; (C) form III; (D) form IV; and (E) form V.

Gas Spectroscopy

Gas absorption spectra



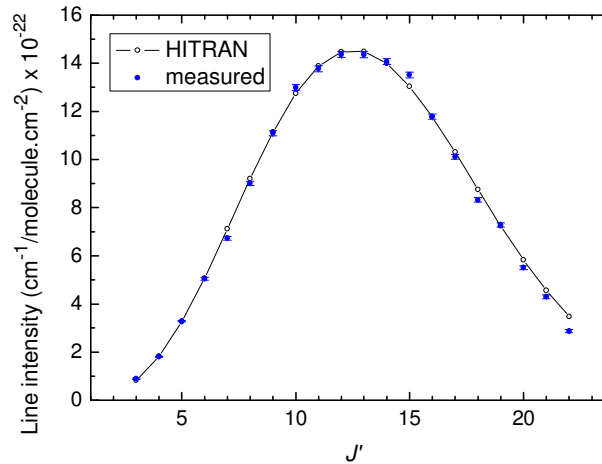
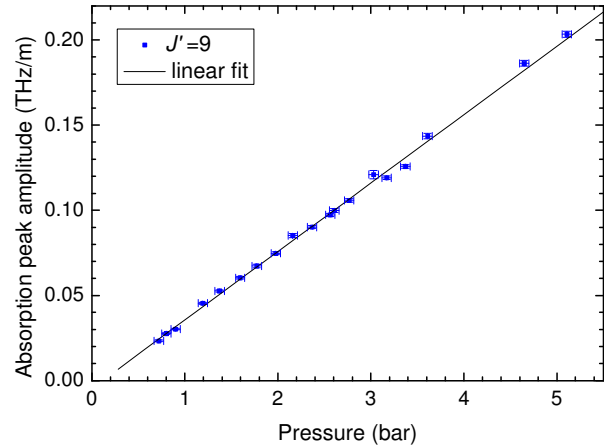
Water vapour



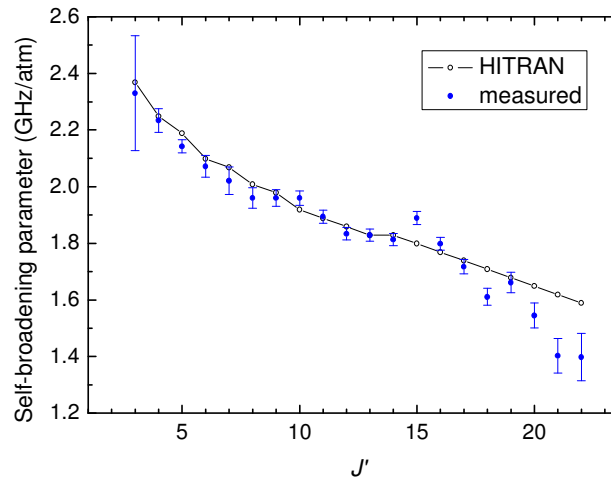
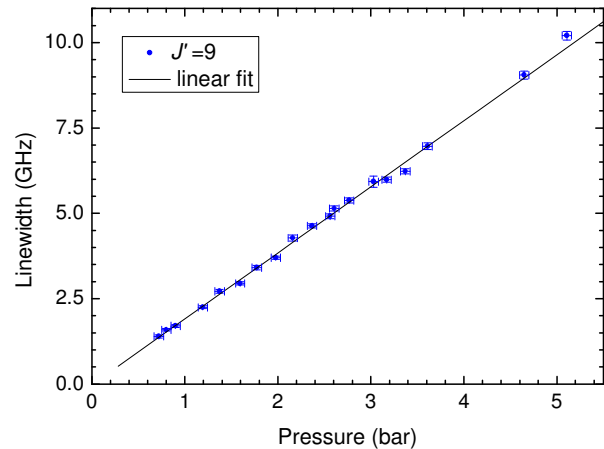
Carbon monoxide

THz TDS is not suitable for high-resolution gas spectroscopy,
due to its low resolution compared with other techniques.

Linestrengths and self-broadening parameters of carbon monoxide



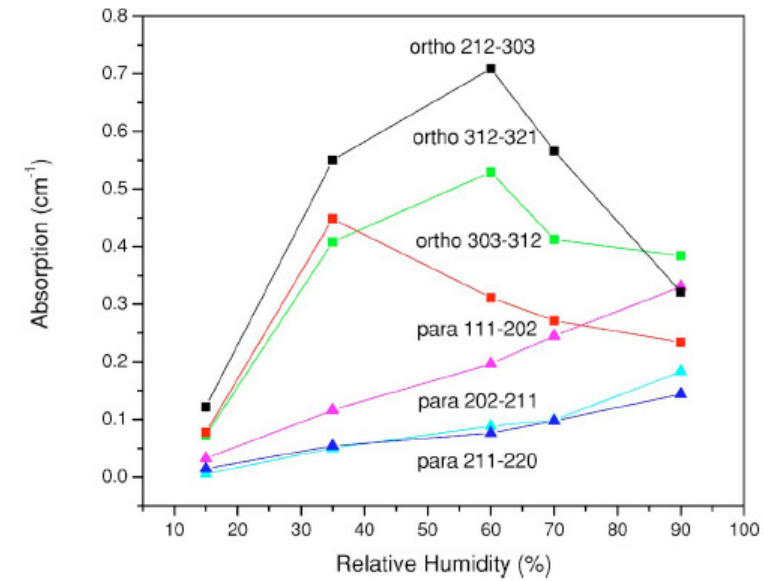
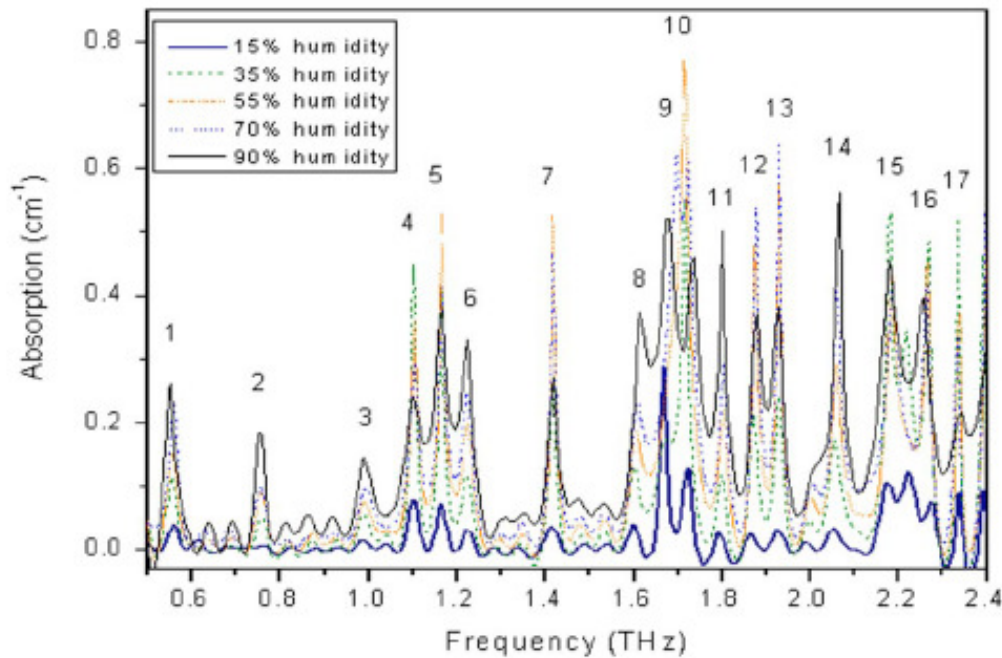
linestrengths



self-broadening
parameters

THz absorption of *para* and *ortho* vapours at different humidities

X. Xin et al, J. Appl. Phys. **100**, 094905 (2006)

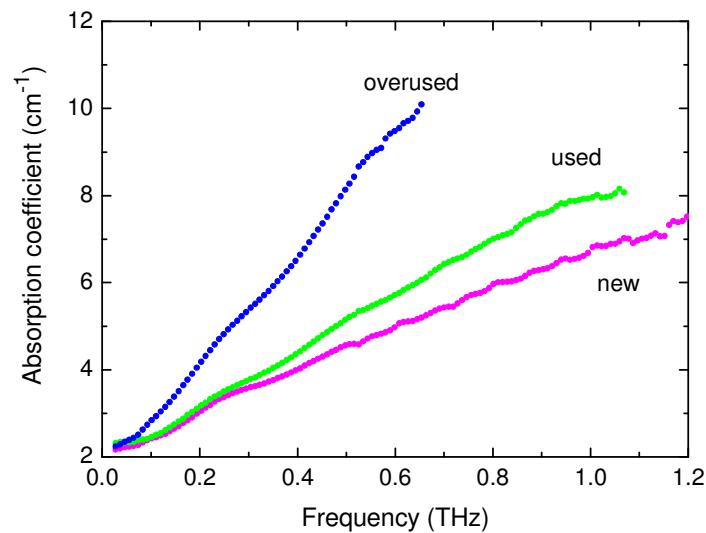
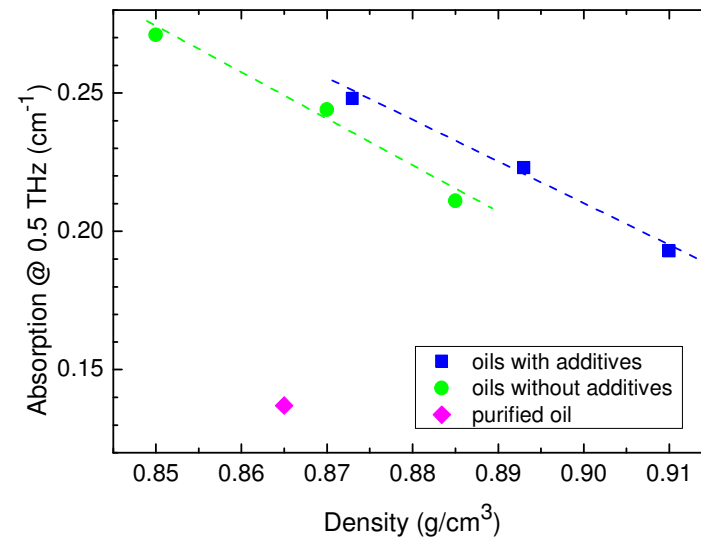
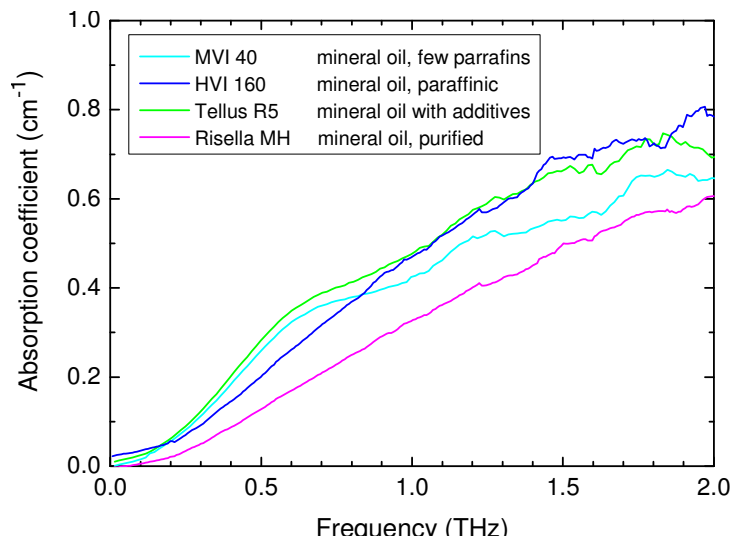


- 212→303: 79.496 cm⁻¹
- 312→321: 173.365 cm⁻¹
- 303→312: 136.76 cm⁻¹
- 111→202: 37.137 cm⁻¹
- 202→211: 70.091 cm⁻¹
- 211→220: 95.176 cm⁻¹

Oils

- Characterising oils
- Relationship with oil properties
- Identifying oil additives
- Observing oil degradation/contamination

Shell Oils



Degradation of engine oil

Oil properties

D Mittleman et al, Am. Chem. Soc. Petroleum Research 48172-AC6

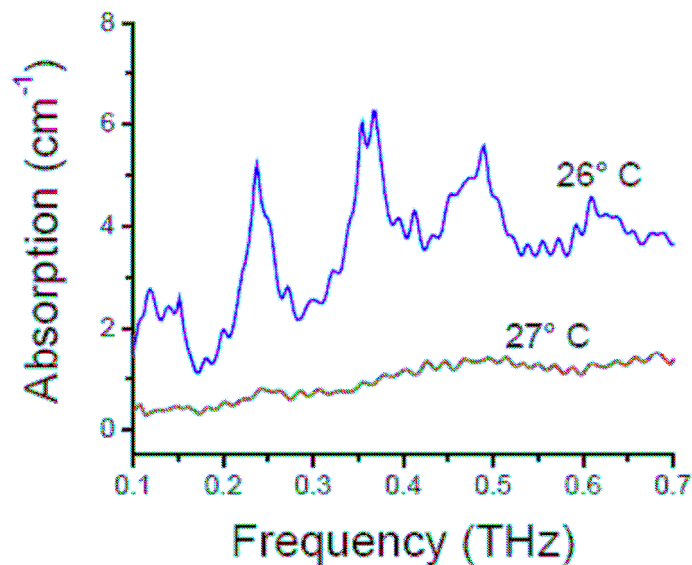


Figure 1 Absorption spectrum of liquid (red) and crystalline (blue) samples of *n*-octadecane. The spectrum of the crystal shows evidence of intermolecular vibrational modes at 0.24 THz, 0.36 THz, and 0.48 THz. The molecular origin of these infrared-active modes is not known.

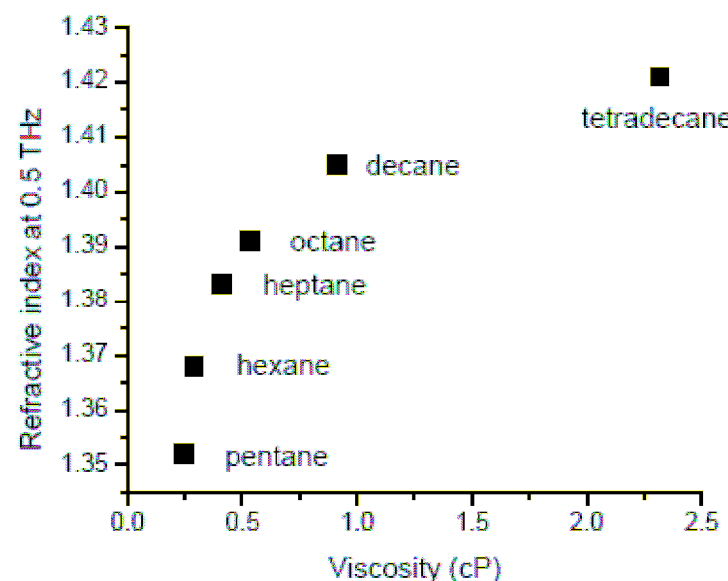
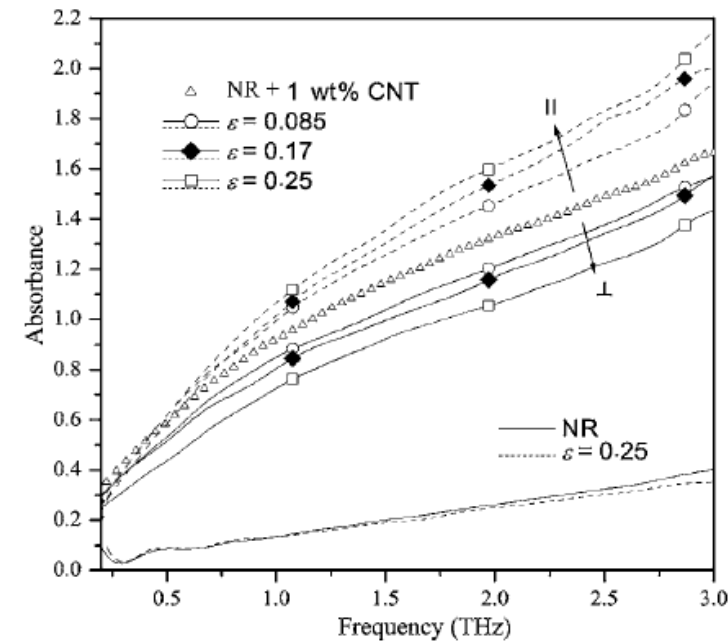
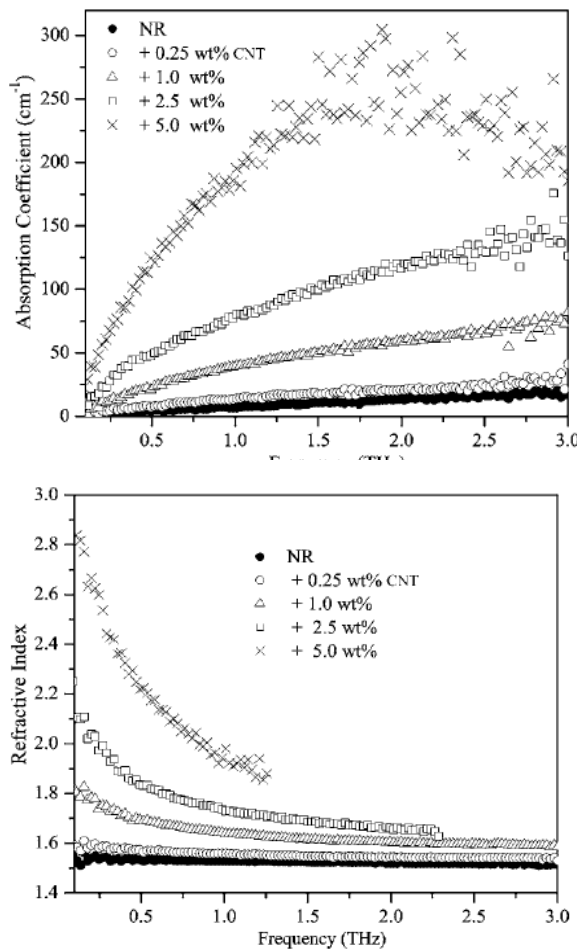


Figure 3 Refractive index of various *n*-alkanes at a frequency of 0.5 THz, as a function of viscosity at room temperature. Viscosity values taken from [46].

Composites

Carbon nanotubes embedded in deformable rubber

R. Rungswang et al., J Appl. Phys. **103**, 123503 (2008)



Strain causes alignment of CNTs

Nondestructive testing of fibreglass aircraft composites

CD Stoik et al, Opt. Express, **16**/21 (2008) 17039

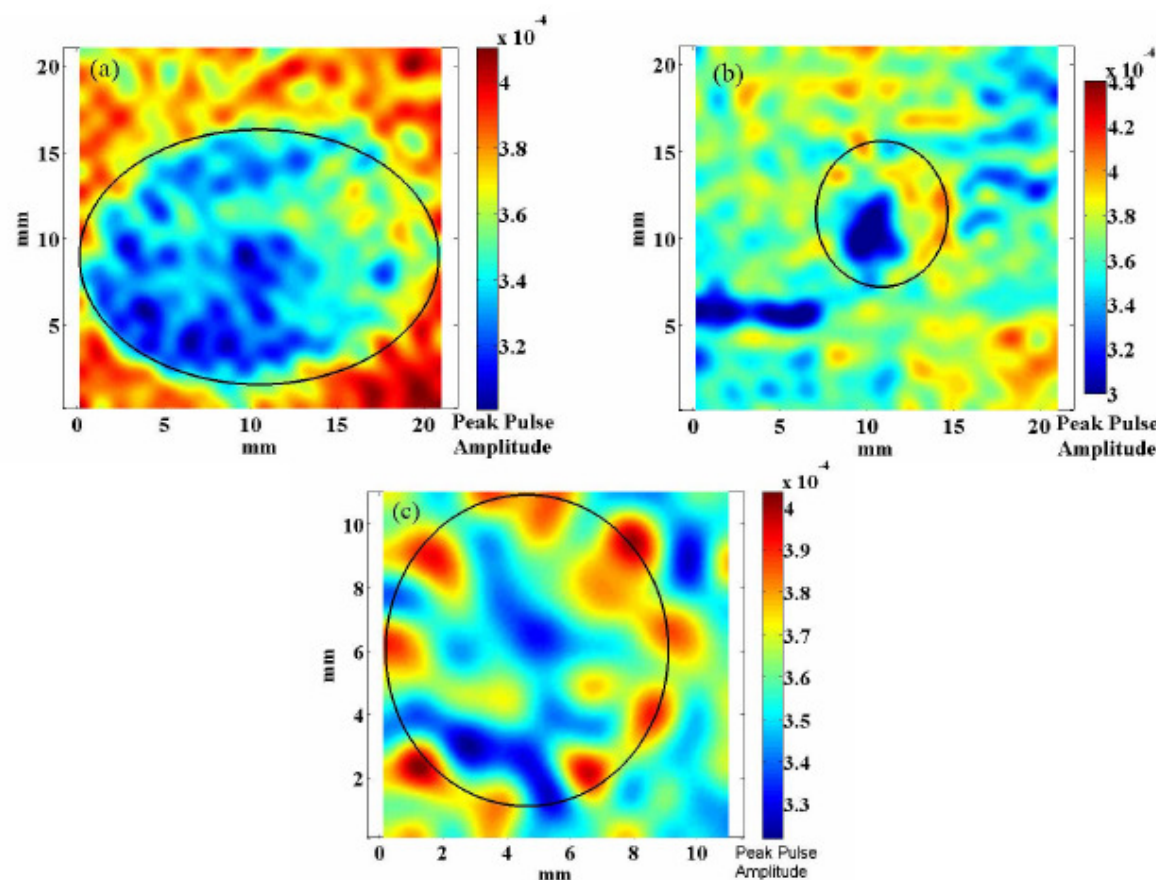


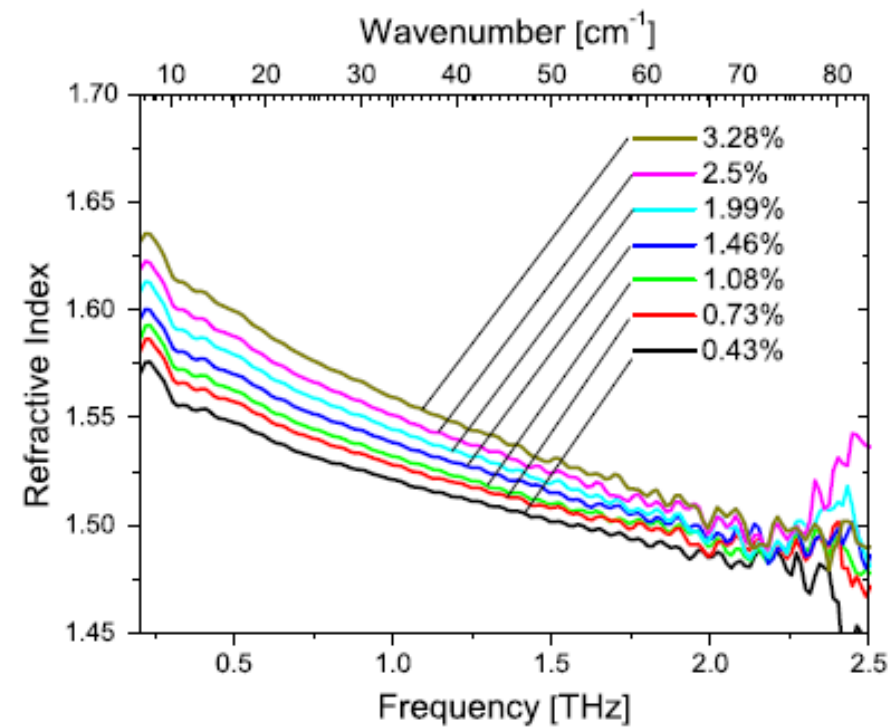
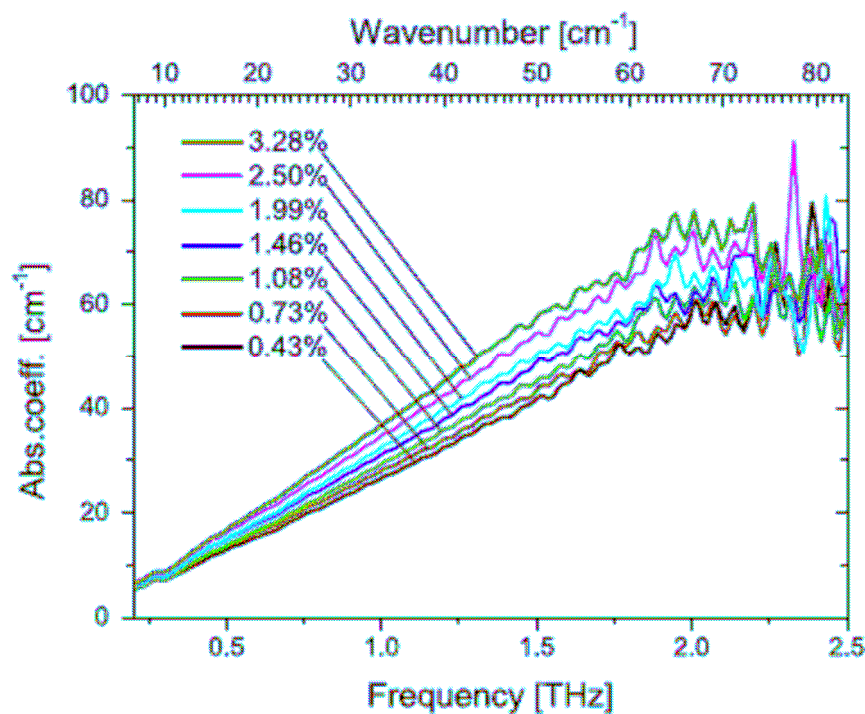
Fig. 8. THz TDS images for three burn areas on glass fiber samples: (a) 440°C for 4 minutes, (b) 430°C for 6 minutes, and (c) 425°C for 20 minutes.

Moisture content of materials

Oil-water complexes of lubricating oils

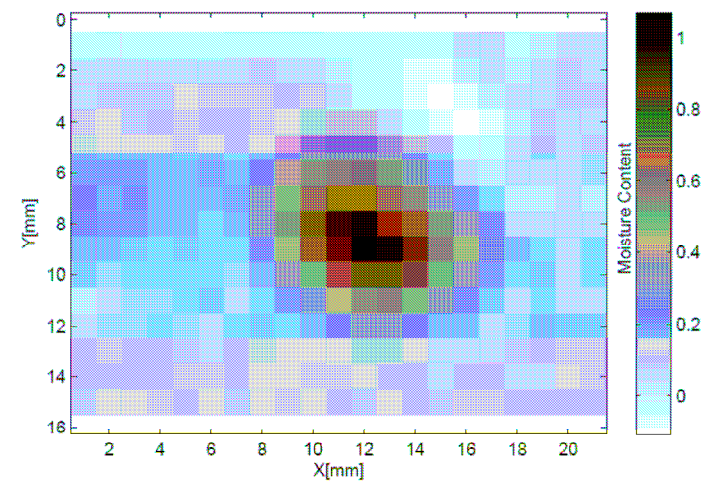
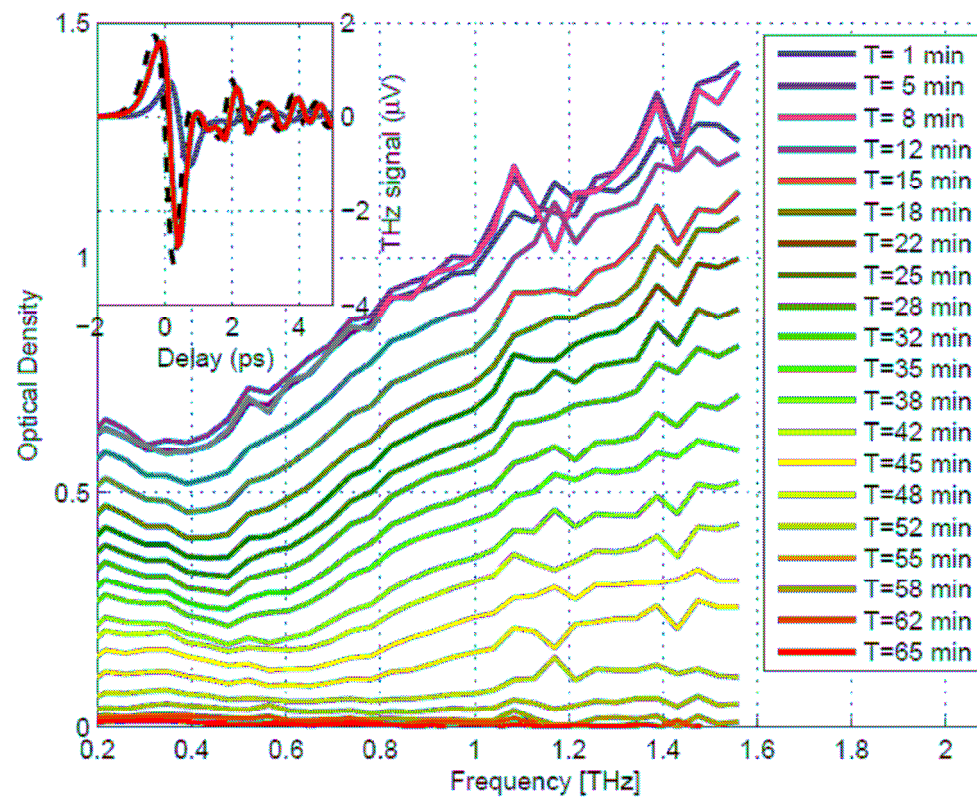
measuring the water content

S. Gorenflo et al, Chem. Phys. Lett. **421** (2006) 494–498



Moisture content of paper

D. Banerjee et al, Opt. Express, **16**/12 (2008) 9060



Measuring the thickness and moisture content of paper

P. Mousavi et al, Appl. Opt. 48/33 (2009) 6541-6546

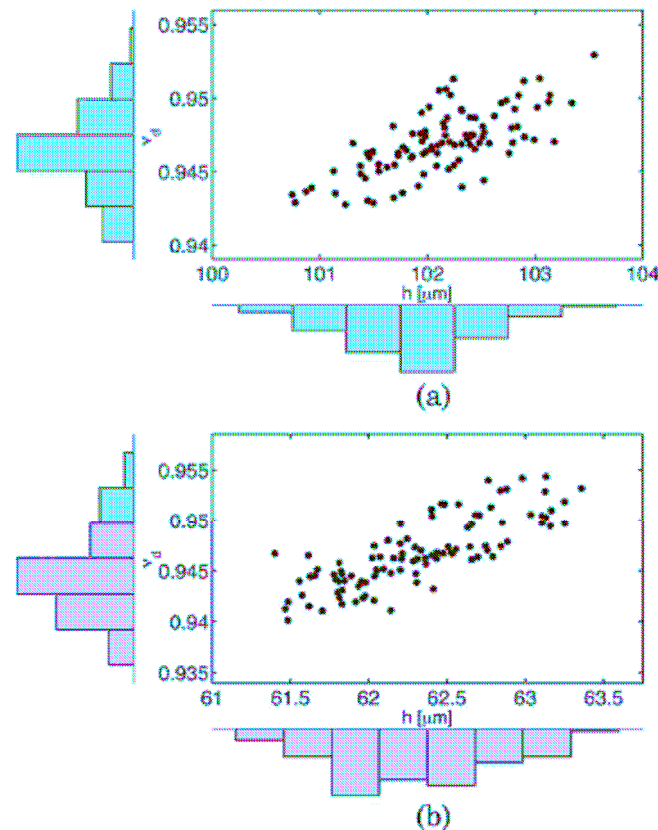


Fig. 3. (Color online) Experimental scatter plots of ν_d and h resulting from repeated THz measurements on the same spot on a sample for (a) photocopy paper and (b) fine paper.

Table 2. Paper Parameters Measured Using THz and by Independent Methods ^a

	THz		Independent	
	h (μm)	M (%)	h (μm)	M (%)
Photocopy	102.12 ± 0.58	6.04 ± 0.25	102.0	5.91
Fine	62.30 ± 0.49	5.47 ± 0.35	62.6	6.44

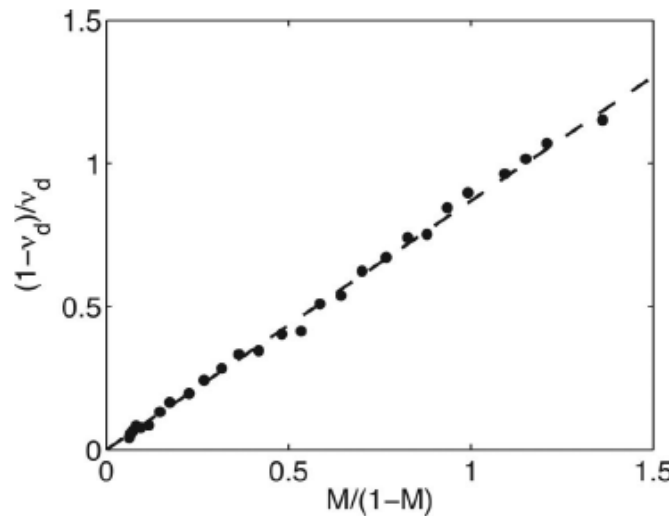
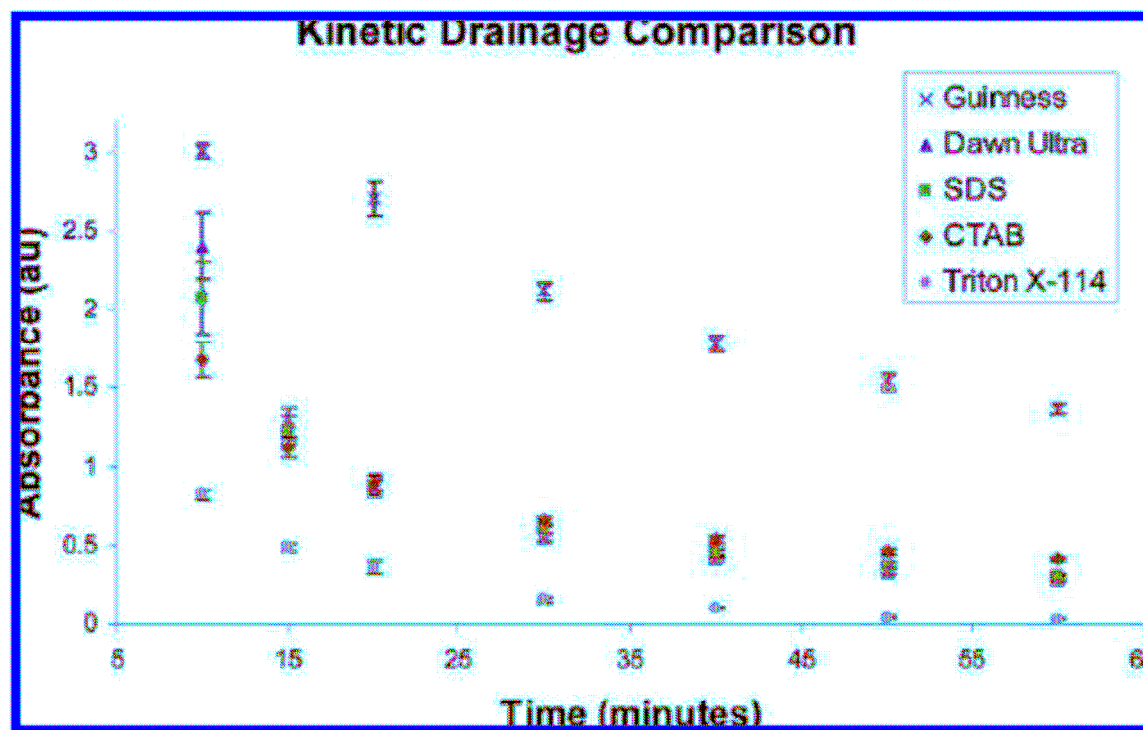


Fig. 2. Calibration of ρ_d/ρ_w . Measurements of moisture fraction M determined by weight are plotted against $\nu_d/(1 - \nu_d)$ determined from THz measurements (●), together with the fit to Eq. (6) with $\rho_d/\rho_w = 0.87$ (dashed line).

Observing aqueous foam drainage

J. Heuser et al, *Langmuir* 2008, 24, 11414-11421



sodium dodecyl sulfate (SDS)
- anionic surfactant
(CTAB) cetyl
trimethylammoniumbromide
– cationic surfactant
Triton X-114
- nonionic surfactant
Ultra Dawn dish soap
- mixed surfactants
Guinness beer
- protein surfactant solution

Conclusion

THz spectroscopy can be applied
in many and varied
areas of research

Think what it can do for you

For more information:

<http://www.npl.co.uk/electromagnetics/terahertz/>

